Pol. J. Environ. Stud. Vol. 34, No. 2 (2025), 1851-1865
DOI: *10.15244/pjoes/188144* ONLINE PUBLICATION DATE: 2024-08-05

Original Research

Synergistic Antifungal Efficiency of Eco-Friendly Synthesized Zinc Oxide Nanoparticles in Combination with Fluconazole against Drug-Resistant Candidal Strains

Mohamed Taha Yassin[1*], Fatimah O. Al-Otibi[1], Khalid Maniah[1], Sara Mohamed[2], Khadiga A. Hasan[3], Aayasha Negi[4], Mohamed Ragab AbdelGawwad[5]

[1]Botany and Microbiology Department, College of Science, King Saud University, P.O. 2455, Riyadh 11451, Saudi Arabia
[2]Botany and Microbiology Department, Faculty of Science, Benha University, Benha 13511, Egypt
[3]Botany Department, Faculty of Science, Mansoura University, Al Mansurah, Egypt
[4]Department of Chemistry, IFTM University, Moradabad, Uttar Pradesh -244102, India
[5]Genetics and Bioengineering, Faculty of Engineering and Natural Sciences, International University of Sarajevo, 71210 Sarajevo, Bosnia and Herzegovina

Received: 18 March 2024
Accepted: 30 April 2024

Abstract

The resistance of fungal pathogens to traditional antifungal medications presents a significant public health concern, particularly for immunocompromised patients, leading to elevated rates of illness and death. This study aimed to explore the antifungal properties of zinc oxide nanoparticles (ZnO NPs) produced using a natural approach involving the aqueous seed extract of *Trigonella foenum-gracium* (Fenugreek). Additionally, the study assessed the combined effectiveness of these biologically synthesized ZnO NPs with fluconazole against fungal pathogens. The biologically synthesized ZnO NPs were observed to have a hexagonal shape with an average diameter of 27 nm and a surface charge of -18.3 mV. Notably, these nanoparticles exhibited the most potent antifungal activity against *Candida tropicalis*, with a relative inhibition zone diameter of 18.67±0.56 mm. The minimum inhibitory concentration against *C. tropicalis* was determined to be 100 µg/mL, while the minimum fungicidal concentration was found to be 200 µg/mL. The greatest synergistic effect between the biologically synthesized ZnO NPs and fluconazole was observed against *Candida glabrata*, followed by *Candida parapsilosis*. In summary, the study underscores the potential of combining biologically synthesized ZnO NPs with fluconazole to formulate an effective antifungal treatment against drug-resistant fungal pathogens, thereby enhancing the therapeutic efficacy of conventional antifungal drugs.

Keywords: green synthesis, *Trigonella foenum-gracium*, synergism, fluconazole, toxicity assay

*e-mail: myassin2.c@ksu.edu.sa
Tel.: +966562137875

Introduction

Invasive fungal infections mostly affect hospitalized and immunocompromised individuals [1]. These infections have a notable mortality rate and are predominantly opportunistic in origin [2]. Treating these infections may be difficult because of the limited selection of antifungal medications and the emergence of resistant strains, which narrow down treatment choices [3]. Furthermore, there are few new antifungal drugs discovered, and there is a lack of research on alternative therapies for human fungal diseases [4]. The commonly used antifungal medications for treating Candida infections are nystatin, ketoconazole, clotrimazole, fluconazole, itraconazole, and amphotericin B [3]. The prevalence of infections is increasing due to the overuse of conventional antifungal medications, leading to the development of resistance in opportunistic fungi [5]. In this context, the *Candida glabrata* strain showed a high level of antifungal resistance to azole antifungal agents such as fluconazole, itraconazole, and clotrimazole antifungal agents, as reported previously [6-8]. Additionally, the antifungal drugs routinely used elicit several adverse effects, such as allergic reactions, immune system suppression, and hypersensitivity [9]. Therefore, it is essential to find novel antimicrobial formulations in order to combat the problem of candidal resistance to antifungal treatments and enhance the efficacy of traditional antifungal therapies [10]. Nanoparticles (NPs) are characterized by their one-dimensional nanosize (1–100 nm) and large surface area [11]. Over the last 10 years, researchers have discovered that metal oxide nanoparticles possess significant promise in the field of nanotechnology due to their notable benefits, including their bigger surface area and smaller size. These characteristics enable them to function more effectively as active components [12]. Zinc oxide nanoparticles (ZnO NPs), a prevalent kind of metal oxide, have found extensive applications in several fields, such as medicine, cosmetics, food packaging, and photocatalysis [13]. Multiple techniques may be used to synthesize ZnO NPs, including sol-gel processing, microemulsion, and homogeneous precipitation [14].

Nevertheless, these approaches are plagued by many drawbacks, including the need for costly procedures, the requirement of chemical capping agents, the use of hazardous chemicals, and significant energy usage [15]. Currently, there is significant interest in using environmentally friendly methods to produce nanoparticles (NPs). These methods not only eliminate the need for high-energy and harmful chemicals, but also provide simplicity and cost-effectiveness [16]. Plants contain a wide range of complex and varied bioactive macromolecules, including saponins, polyphenols, and terpenoids. Plant extracts may be used as both stabilizers and reducing agents during the production of nanomaterials [17].

Furthermore, the use of plant extracts in the production of green synthesized ZnO NPs offers exceptional biocompatibility, making them very suitable for many applications [18]. A previous study demonstrated the green synthesis of ZnO nanoparticles utilizing a leaf extract from *Lycopersicon esculentum* and reported the antifungal efficacy of these nanoparticles against *Candida albicans*, a very common fungal pathogen, at a dosage of 100 µg/ml [19]. In a different study, eco-friendly ZnO nanoparticles were synthesized from *Costus pictus* leaf extract. These nanoparticles showed promising antifungal effects against *Aspergillus niger* and *C. albicans strains* [20]. In a comparable study conducted by Irshad et al., ZnO nanoparticles were produced using green tea leaves, and their biocidal ability against *A. niger* was confirmed using the well diffusion technique. Both investigations demonstrated that the negatively charged cell membrane and positively charged nanoparticles are attracted to each other by electrostatic forces. As a consequence, the nanoparticles get attached to the cell membrane, leading to the rupture of the membrane and eventually causing cell death [21]. Fenugreek, scientifically known as *Trigonella foenum-gracium* L., is a plant belonging to the Leguminosae family [22]. The seeds and leaves of Fenugreek plants have hypoglycemic properties as well as antibacterial, anthelmintic, antipyretic, and anti-inflammatory activities [23]. The previous studies have mostly concentrated on the eco-friendly production of biogenic ZnO nanoparticles and examining their antifungal activity. However, there is a scarcity of research on the combined antimicrobial activity of ZnO NPs with antifungal agents. Consequently, the present study focused on the green phytosynthesis of ZnO NPs using an aqueous extract from *T. foenum-graecum* seeds. The study investigated the antifungal properties and synergistic effects of biogenic ZnO NPs against four candidal pathogens: *Candida albicans*, *C. parapsilosis*, *C. glabrata*, and *C. tropicalis.* The cytotoxic impact of biogenic ZnO NPs on normal lung fibroblast cells was examined to assure their biosafety for application.

Materials and Methods

Preparation of Water Extracts of Fenugreek Seeds

The *T. foenum-gracium* seeds were procured from a local market in Riyadh, Saudi Arabia, and were initially identified and deposited by the Herbarium of the Botany and Microbiology Department, assigned the voucher number KSU-202456. To prepare them, the Fenugreek seeds underwent two rounds of washing with tap water, followed by two rounds of rinsing with distilled H_2O, and were then thoroughly dried in a shaded area. The dried seeds were crushed into a consistent powder using a mechanical mortar. Subsequently, 50 grams of the powdered plant material were added to 500 mL flasks containing 200 mL of deionized water. The mixture was heated on a hot plate at 50ºC for 30 minutes. Placed on a magnetic stirrer, the flasks were incubated at 25ºC

for 24 hours. Afterward, the extracts were filtered using Whatman filter paper (grade 1) and then sterilized through filtration using a 0.22 µm Millipore membrane filter. The resulting aqueous solution from Fenugreek seeds was preserved at 4ºC for future utilization [24, 25].

Biogenic Synthesis of ZnO NPs

A total of 5 mL of fenugreek seed extract was gradually added to a solution containing 95 mL of zinc nitrate hexahydrate (0.01 M). The Zn^{2+} and seed extract were vigorously mixed together and stirred continuously at room temperature for 1 hour. This was done to facilitate the electrostatic interaction between the Zn^{2+} ions and the biomolecules present in the seed extract. The pH of the mixture was later adjusted to 12 by adding NaOH (0.02 M) and stirring continuously using a magnetic stirrer for 2 hours at 60ºC. The result was a solution with a yellowish-white color. A centrifugation process was used to separate a white ZnO powder at 10000 rpm for 20 min. The powder was subjected to two washes using distilled H_2O, followed by three rinses with 100% ethanol to eliminate contaminants. Finally, it was dried overnight at 60ºC in an oven. Afterward, the dried zinc oxide nanoparticles were subjected to calcination in a muffle furnace at a temperature of 400ºC for a duration of 2 hours [26].

Characterization of the Biogenic ZnO NPs

The optical features of ZnO NPs were assessed using an Ultraviolet-Visible Spectrometer within a wavelength range of 200 nm - 800 nm. The morphology and average nanosize of ZnO NPs were determined through transmission electron microscopy. Elemental composition and mapping were examined using an energy-dispersive X-ray (EDX) analyzer, while Fourier transform infrared spectroscopy was employed to identify the main functional groups of ZnO NPs. The crystalline characteristics and size were analyzed using a Shimadzu XRD model 6000 diffractometer with Cu K-alpha radiation (wavelength: 1.5402 Å). The average diameter in colloidal solutions and surface charge were detected using Zeta sizer equipment.

Screening of the Antifungal Effectiveness of Biogenic ZnO NPs

Adisc diffusion assay was used to evaluate the antifungal activity of the biogenic ZnO NPs against four candidal strains, namely *Candida albicans* (ATCC 90028), *C. parapsilosis* (ATCC 22019), *C. glabrata* (ATCC 90876), and *C. tropicalis* (ATCC 13803). The isolates were cultured on Sabouraud dextrose agar medium (SDA) at 28ºC overnight to obtain fresh inoculums. A 100-µL candidal suspension of each strain was transferred onto freshly prepared SDA plates and spread homogenously using sterile swabs. The desiccated ZnO nanoparticles were dissolved in methanol and subjected to sonication to ensure thorough uniformity of the sample. Discs of filter paper measuring 8 mm in diameter were impregnated with 100 and 200 µg of ZnO NPs. Discs of filter paper soaked just in methanol solvent were used as negative controls. The positive control discs consisted of fluconazole at a concentration of 25 µg, which were then put on top of the seeded SDA medium. Afterwards, the plates were placed in an incubator set at a temperature of 35ºC for a duration of 48 hours. Following this, the diameters of the inhibitory zones were measured using a Vernier caliper. The biogenic ZnO NPs were evaluated for their minimum inhibitory concentration (MIC) against *C. tropicalis*, which exhibited the greatest susceptibility to the ZnO-NPs. The broth microdilution experiment was conducted in 96-well microtiter plates, following the methodology published in a previous study [27]. In addition, the minimum fungicidal concentration (MFC) was determined by streaking the concentration that inhibits the growth of fungi (MIC) and the two following concentrations on freshly produced SDA plates. The plates were thereafter placed in an incubator set at a temperature of 35ºC for a period of 24 hours. The MFC concentration is the minimum concentration at which no fungal growth was detected.

Synergistic Antifungal Activity of Biogenic ZnO NPs with Fluconazole

The biogenic ZnO NPs at a concentration of 200 µg/disk showed antifungal proficiency against the concerned strains. Therefore, the effectiveness of the biogenic ZnO NPs (200 µg) in combination with fluconazole (25 µg) against the tested strains was evaluated using a disc diffusion experiment to determine their synergistic antifungal properties. Positive controls were created using filter paper discs that were impregnated with fluconazole (25 µg), whereas negative controls were made by filling the discs with methanol solvent. In addition, an additional set of filter paper discs was loaded with a combination of fluconazole and ZnO nanoparticles to investigate their combined effect. Ultimately, paper discs that were treated with 200 µg of biogenic ZnO NPs were compared to discs treated with fluconazole and ZnO NPs. The loaded discs were positioned on the SDA plates previously inoculated and prepared as described earlier, followed by an incubation period of 48 hours at 35ºC. The inhibitory zones were gauged using a Vernier caliper, and the increase in the fold of inhibition area (IFA) was quantified based on the provided Equation (1).

$$IFA = (B^2 - A^2)/A^2 \quad (1)$$

where B and A represent the inhibition zone diameters for the combination of fluconazole + ZnO-NPs and fluconazole antifungal alone, respectively.

Investigation of Fungal Cell Deformations Using SEM Analysis

The SEM analysis was employed to assess the morphological alterations in fungal cells treated with biogenic ZnO NPs. The agar sections from the inhibition zones were extracted and immersed in a solution with 3% (v/v) glutaraldehyde, buffered with 0.1 M sodium phosphate at a pH of 7.2, for 60 minutes at 25ºC. Following this, the agar pieces underwent four rinses in a buffer solution and were then post-fixed in a 1% (w/v) osmium tetroxide (OsO4) solution for 1 hour. The samples underwent alcoholic dehydration, being immersed in ethanol solutions ranging from 30% to 100% for 15 minutes. After complete drying, the specimens were affixed to stubs using double-sided carbon tape. A thin layer of gold coating was applied using a Polaron SC 502 sputter coater, and the morphological alterations were observed using a scanning electron microscope (JEOL JSM-6380 LA).

Cytotoxicity Assay

The toxicity of ZnO NPs, synthesized with *T. foenum-gracium* seed extract, against the WI-38 cell line (normal lung fibroblast cells), was assessed through the methylthiazolyl diphenyl-tetrazolium bromide (MTT) test. Various concentrations of ZnO NPs (25, 50, 100, 200, 400, 800, and 1600 µg/mL) were tested. Each well of a 96-well tissue culture plate received a cell concentration of 1 x 10^5 cells/mL in a volume of 100 µL. The plate was then incubated at 37ºC for 24 hours, and after removing the growth media, biogenic ZnO NPs were cultured in RPMI media with 2% serum, undergoing serial dilutions. Each well was treated with 0.1 mL of each dilution, with three control wells receiving only serum. Following a 48 hour incubation at 37ºC, a 5 mg/mL MTT solution in PBS was prepared. Each well was treated with 8-20 µL of the MTT solution, agitated for 5 minutes, and maintained at 37ºC with 5% CO_2 for 4 hours until formazan formation occurred. The formazan was then dissolved in 200 µL of dimethyl sulfoxide (DMSO) with gentle agitation for 5 minutes. Absorbance was measured at 560 nm, and the IC_{50} value was determined using linear regression analysis to identify the concentration of biogenic ZnO NPs resulting in a 50% reduction in cell viability.

Statistical Analysis

The analysis of the data was conducted utilizing GraphPad Prism version 8.0 (GraphPad Software, Inc., La Jolla, CA, USA), employing the Tukey test within a one-way ANOVA at a significance level of 0.05. The experimental methods were performed in triplicate, and the results were given as the mean value±standard error. OriginPro 2018 was used to draw the particle size distribution histogram and XRD patterns.

Results and Discussion

Green Biofabrication of ZnO NPs

Phytochemicals, such as polyphenols, sugars, proteins, alkaloids, phenolic acids, carboxylic acids, saponins, carbohydrates, and terpenoids, are crucial in the process of reducing and stabilizing metal nanoparticles because of their ability to cap them [28]. The stabilizers or agents that stabilize the seed extract of *T. foenum-graecum* interact with the bio-reduced zinc atoms in order to enhance the stability of the nanoparticles and prevent their further agglomeration [29]. The process by which ZnO NPs are formed in this context is depicted in Fig. 1a), wherein the active phytochemicals function as reducing agents to transform zinc ions into elemental zinc, which subsequently reacts with oxygen to form ZnO NPs. Additionally, they act as capping agents, which enhance the stability of the biogenic ZnO NPs and prevent particle aggregation. Fig. 1b) shows the formation of biogenic ZnO NPs as a yellowish-white solution after the addition of the plant extract to a colorless zinc nitrate hexahydrate solution and adjusting the pH of the solution to 12.

Characterization of the Biogenic ZnO NPs

UV Spectral Analysis of ZnO NPs

The optical characteristics of ZnO NPs were examined using UV analysis. The UV spectra of both ZnO NPs and Fenugreek seed extract exhibited a UV peak at 250 nm, indicating that the phytochemicals in the extract serve as reducing and capping agents for ZnO NPs (Fig. 2a). The extract's spectra showed a broad absorption range spanning from 365 nm to 800 nm, with a maximum of 517 nm. Conversely, the spectra of ZnO NPs exhibited a displacement towards a longer wavelength, with a maximum of 554 nm. The shift may be ascribed to the surface plasmon resonance (SPR) of ZnO NPs. The band gap energy of ZnO NPs was appraised using the Tauc plot approach and detected to be 3.15 eV, as seen in Fig. 2b). The findings of our investigation were in alignment with a prior publication that displayed the environmentally friendly synthesis of ZnO NPs utilizing *Eucalyptus leaves*. The nanoparticles were found to have a band gap energy of 3.15 eV [30]. The findings were further confirmed by previous work that demonstrated the eco-friendly production of ZnO NPs using sawdust. This process yielded biogenic nanoparticles with a band gap energy of 3.15 eV [31].

Morphology and Particle Size Distribution of Bioinspired ZnO NPs

An investigation using a transmission electron microscope (TEM) was performed to identify the shape and size distribution of ZnO NPs. TEM analysis demonstrated that ZnO NPs had a hexagonal

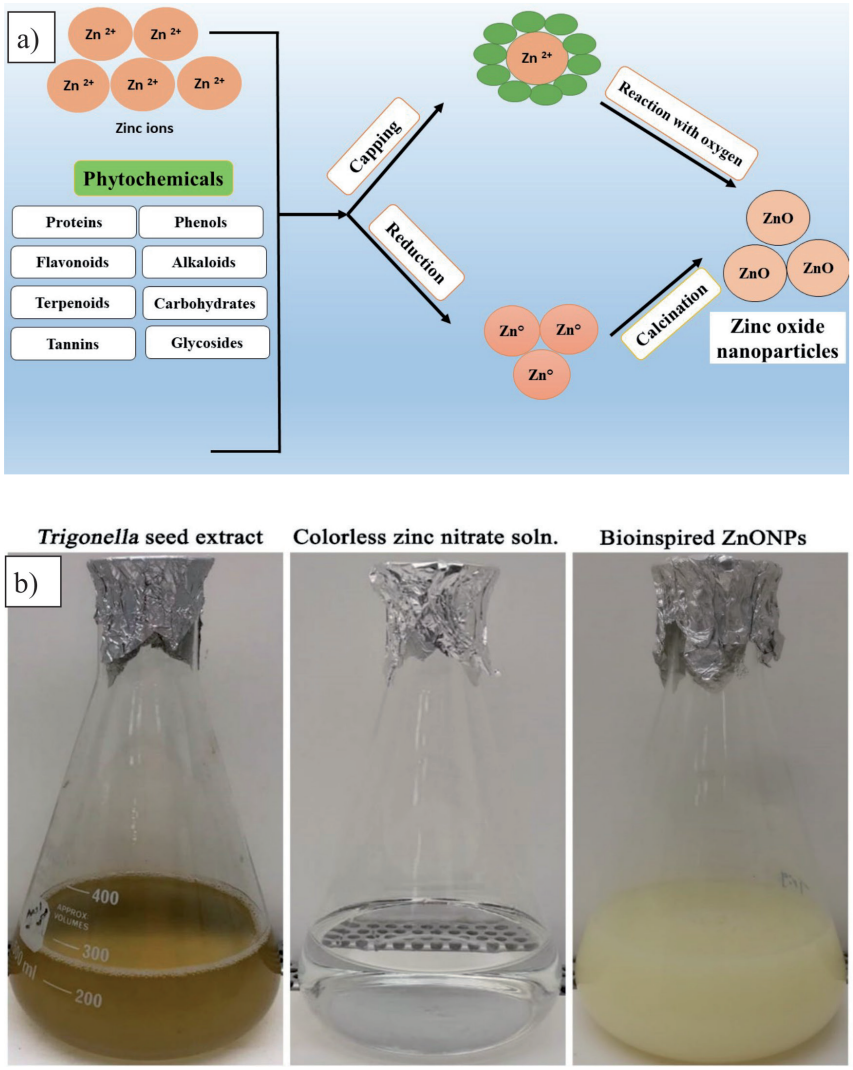

Fig. 1. a) Mechanistic formation of ZnO NPs with the water seed extract of *T. foenum-graecum,* b) Reduction of the colorless $Zn(NO_3)_2 \cdot 6H_2O$ solution with *T. foenum-graecum* extract.

morphology, as seen in Fig. 3a). The mean particle diameter, as derived from the particle size distribution histogram shown in Fig. 3b), was 27.92 nm. A prior investigation documented the eco-friendly production of ZnO NPs through the utilization of *Brassica oleracea* var. *italica* extract. The average size of the particles, as determined by TEM examination, was found to be 47 nm [32]. The ZnONPs, synthesized using a leaf extract derived from *Ipomoea aquatica*, exhibited an average particle size of 67.70 nm, as reported in a prior investigation [33]. The phytosynthesized ZnO NPs obtained in this work were smaller compared to previous research, which confirms the success of the adopted green synthesis method.

EDX Analysis of the Bioinspired ZnO NPs

The elemental composition of the bioinspired ZnO NPs was investigated using EDX analysis. The EDX spectrum confirmed the presence of ZnO NPs based on the elemental mapping, which revealed the existence of zinc and oxygen with mass percentages of 51.42% and 48.58%, respectively (Table 1). Fig. 4 demonstrated the existence of an oxygen peak at 0.525 keV, whereas the presence of zinc was indicated by the prominent peaks seen at 1.1, 8.6, and 9.5 keV, corresponding to Zn *Lα,* Zn *Kα*, and Zn *Kβ*, respectively. The results of our investigation align with previous research that demonstrated the environmentally friendly production of ZnO NPs using *Borassus flabellifer* fruit extract. Our analysis also confirmed the existence of prominent peaks at energy levels of 0.5 keV, 1.1 keV, 8.6 keV, and 9.5 keV, which correspond to O K, Zn L, Zn K, and Zn Kβ, respectively [34].

FTIR Analysis of the Greenly Synthesized ZnO NPs

Fourier transform infrared spectroscopy (FTIR) analysis of *T. foenum-graecum* extract showed the presence of 7 bands at wavelengths of 3431.76, 2079.17, 1637.38, 1387.18, 1310.82, 1111.54, and 668.75 cm^{-1} (Table 2). Furthermore, the FTIR spectra of ZnO NPs

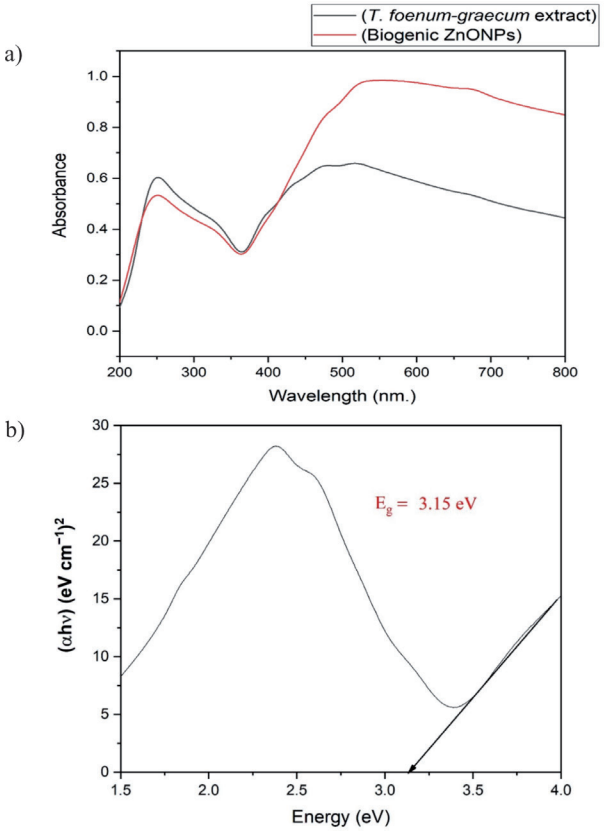

Fig. 2. a) UV analysis of *T. foenum-graecum* extract and the biogenic ZnO NPs, b) Band gap energy of ZnO NPs.

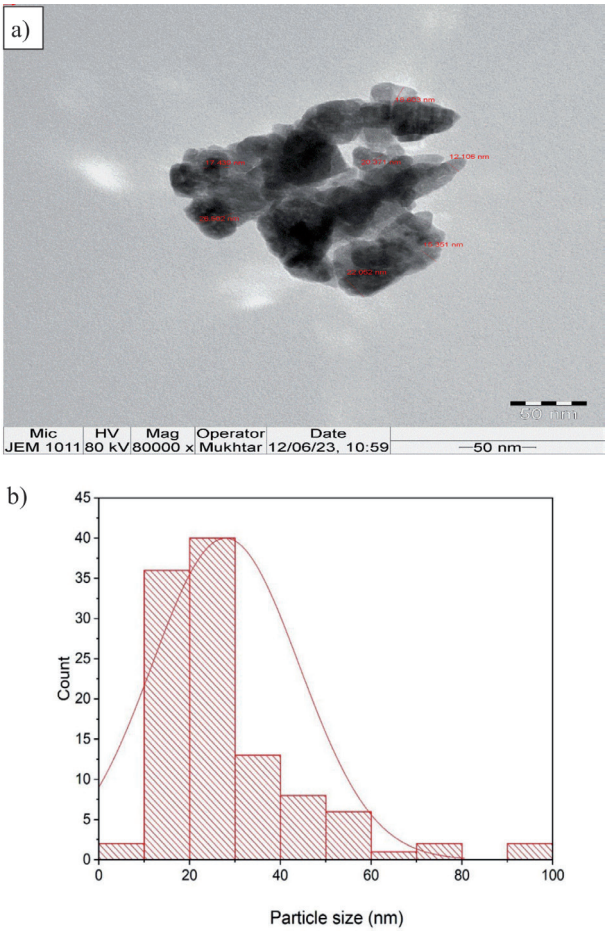

Fig. 3. a) TEM graph of the bioinspired ZnO NPs, b) Particle size distribution histogram of ZnO NPs.

exposed the existence of eleven absorption bands at 3414.20, 2929.26, 2376.10, 2077.71, 1628.53, 1491.58, 1394.99, 1037.16, 904.91, 645.61, and 550.22 cm^{-1} (Fig. 5). The absorption bands detected at 3431.76 and 3414.20 cm^{-1} detected at the spectra of *T. foenum-graecum* extract and ZnO NPs, respectively, could be allocated to the O-H stretching of phenolic compounds [35, 36]. In this context, the data confirmed the role of the phenolic constituents of the water seed extract as reducing and capping agents for ZnO NPs. Moreover, the absorption band at 2079.17 cm^{-1} in the spectra of the aqueous extract of *T. foenum-graecum* was shifted to a lower wavelength in the spectra of ZnO NPs at 2077.71 cm^{-1}, indicating N=C=S stretching of isothiocyanate functional groups [37]. The two absorption bands found in ZnO NPs spectra at 2929.26 and 2376.10 cm^{-1} could be allotted to C-H and N–H stretching of alkanes and amines, respectively. In this setting, the extracted biomolecules, such as amines and alkanes, are capped over the surface of ZnO NPs, contributing to their stability and preventing their agglomeration. In addition, the band seen in the spectra of the plant extract at 1637.38 cm^{-1} was shifted to a lower wavelength at 1628.53 cm^{-1} in the IR spectra of ZnO NPs. This shift indicates that the C=C stretching of alkenes and the capping of alkenes over ZnO NPs surface [38]. Nevertheless, the band observed at 1387.18 cm^{-1} in the FTIR spectra of the seed extract of *T. foenum-graecum* was shifted to a higher wavelength at 1394.99 cm^{-1} in the spectra of bioinspired ZnO NPs. This shift indicates the O-H bending of alcoholic compounds and suggests that these biomolecules play a role in capping these ZnO NPs [39]. Furthermore, the amine functional group was observed in the spectra of the biogenic ZnO NPs at a wavelength of 1037.16 cm^{-1} due to C-N stretching [40]. The new band formed in the spectra of the biogenic ZnO NPs at 550.22 cm^{-1} was assigned to metal oxide bonds, affirming the formation of ZnO NPs [41].

XRD Analysis of the Bioinspired ZnO NPs

Eleven diffraction peaks were detected in the XRD spectrum of ZnO NPs at two theta angles: 32.01º, 34.56º, 36.45º, 47.73º, 56.63º, 62.89º, 66.58º, 68.08º, 69.31º, 72.64º, and 77.09º. The specific diffraction lattice planes

Table 1. Elemental composition of the biogenic ZnONPs.

Elements	(keV)	Mass%	Atomic %
O K	0.525	48.58	79.42
Zn K	8.630	51.42	20.58

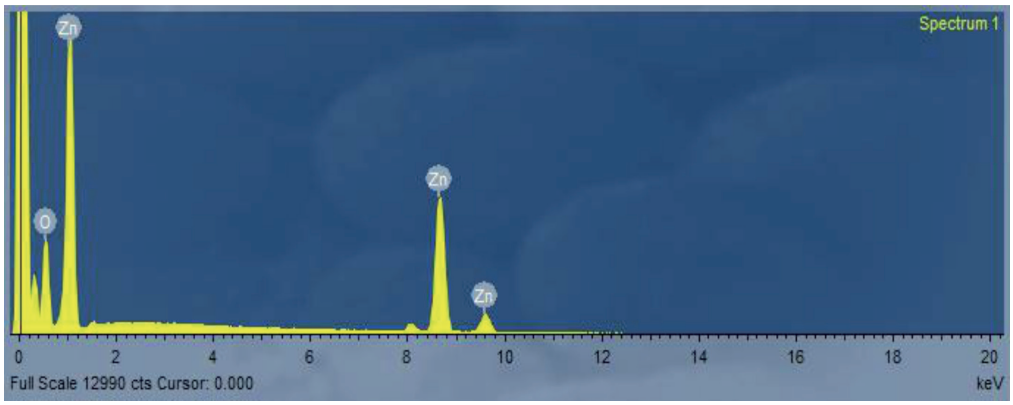

Fig. 4. Elemental map of ZnO NPs.

Table 2. Functional groups of the biogenic ZnONPs and the water extract of *Trigonella foenum-graecum*.

	T. foenum-graecum extract			
No.	Absorption Peak (cm^{-1})	Appearance	Functional Groups	Molecular Motion
1	3431.76	Strong, broad	Alcohols and phenols	O-H stretching
2	2079.17	Medium	Isothiocyanate	N=C=S stretching
3	1637.38	Strong	Alkenes	C=C stretching
4	1387.18	Medium	Alcohols	O-H bending
5	1310.82	Weak	Phenols	O-H bending
6	1111.54	Medium	Secondary alcohol	C-O stretching
7	668.75	Strong	Alkenes	C=C bending
Biogenic ZnONPs				
1	3414.20	Strong, broad	Alcohols and phenols	O-H stretching
2	2929.26	Medium	Alkanes	C-H stretching
3	2376.10	Weak	Amines	C=O or N–H stretching
4	2077.71	Weak	Isothiocyanate	N=C=S stretching
5	1628.53	Medium	Conjugated alkene	C=C stretching
6	1491.58	Medium	Aromatic compounds	C=C stretching
7	1394.99	Medium	Alcohols	O-H bending
8	1037.16	Medium	Amines	C-N stretching
9	904.91	Medium	Alkenes	C=C bending
10	645.61	Weak	Alkyl halides	C-Cl stretching
11	550.22	Medium	Metal oxide bonds	Zn-O stretching

denoted by these peaks were as follows: (100), (002), (101), (102), (110), (103), (200), (112), (201), (004), and (202), respectively, (Fig. 6). The crystalline nanosize of ZnO NPs was detected using Scherrer's Equation (2).

$$D = (k\lambda/\beta \cos \theta) \quad (2)$$

Where λ denotes the X-ray wavelength (1.54178 Å), k signifies Scherrer's constant (k = 0.94), θ signifies the diffraction angle (36.35º), and β signifies the full width at half maximum (FWHM) of the most intense diffraction peak (0.6791). The crystalline nanosize of ZnO NPs was detected to be 12.87 nm. Our outcomes were in line with those of a prior study that proved the phytosynthesis of ZnO NPs using the leaf extract of *Callicarpa tomentosa* with XRD spectra of diffraction peaks at 2 theta angles of 32.71, 35.91, 38.15, 47.98, 57.05, 63.22, 66.71, 67.86, 69.27, 73.52, and 77.84, corresponding to the Bragg

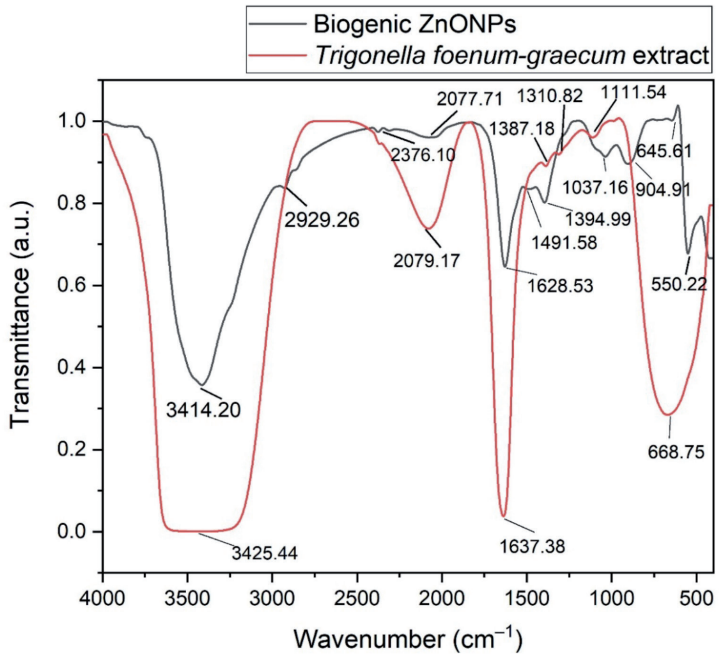

Fig. 5. FTIR spectrum of both of the water seed extract of *T. foenum-graecum* and the biogenic ZnO NPs.

reflection peaks of (100), (002), (101), (102), (110), (103), (200), (112), (201), (004), and (202), respectively [42]. XRD analysis confirmed that the ZnO NPs had a hexagonal wurtzite crystal structure, according to JCPDS file no. 89-7102 [42].

Zeta Potential Analysis of the Biogenic ZnO NPs

The bioinspired ZnO NPs have an average hydrodynamic diameter of 169.6 nm, as shown in Fig. 7a). This measurement is larger than what was detected through XRD and TEM analysis because the nanoparticles in the solution tend to agglomerate due to the presence of plant biomolecules. Additionally, the dynamic light scattering technique measures not only the diameter of the bioinspired ZnO NPs but also the additional hydrate layer surrounding them [43]. Besides, ZnO NPs were determined to have a surface charge of –18.3 mV (Fig. 7b). This suggests that the surfaces of the nanoparticles are capped with molecules that consist mostly of negatively charged groups. These charged groups contribute to the stability of the nanoparticles [44]. The results of our study align with a recent publication that demonstrated the environmentally friendly production of ZnO NPs using an extract derived from *Sesamum indicum* L. seeds. The zeta potential value of ZnO NPs was evaluated to be -18.3 mV [45]. The presence of a negative charge on the surface of ZnO NPs leads to repulsion between the bioinspired ZnO nanoparticles. This repulsion contributes to the stability of nanoparticles in colloidal solutions [46].

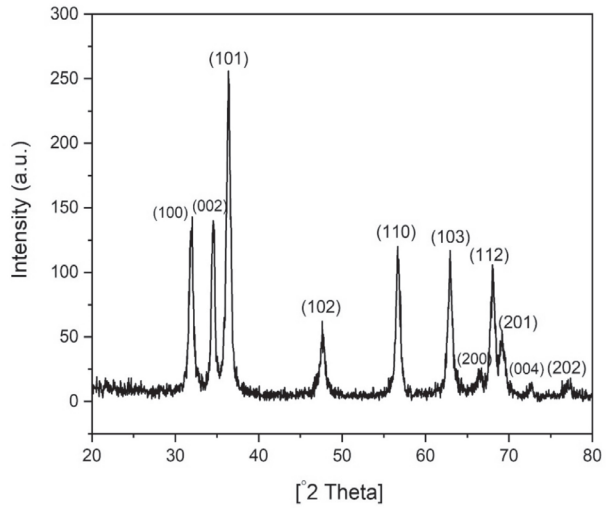

Fig. 6. XRD pattern of ZnO NPs.

Assessment of the Antifungal Proficiency of ZnO NPs

The antifungal effectiveness of ZnO NPs was evaluated against candidal infections. Within this particular framework, the findings indicated that *C. tropicalis* exhibited the highest level of susceptibility to phytosynthesized ZnO NPs. The inhibitory zone diameter was measured to be 18.67±0.56 mm when the concentration of ZnO NPs was 200 µg/disk (Table 3). In addition, the biogenic ZnO NPs exhibited anticandidal effects on the tested pathogens at a concentration of 100µg, except for the *C. glabrata* strain. However, at a concentration of 200 µg/disk, the biogenic ZnO NPs demonstrated antifungal activity against *C. glabrata*, resulting in an inhibitory zone diameter of 10.61±0.47 mm.

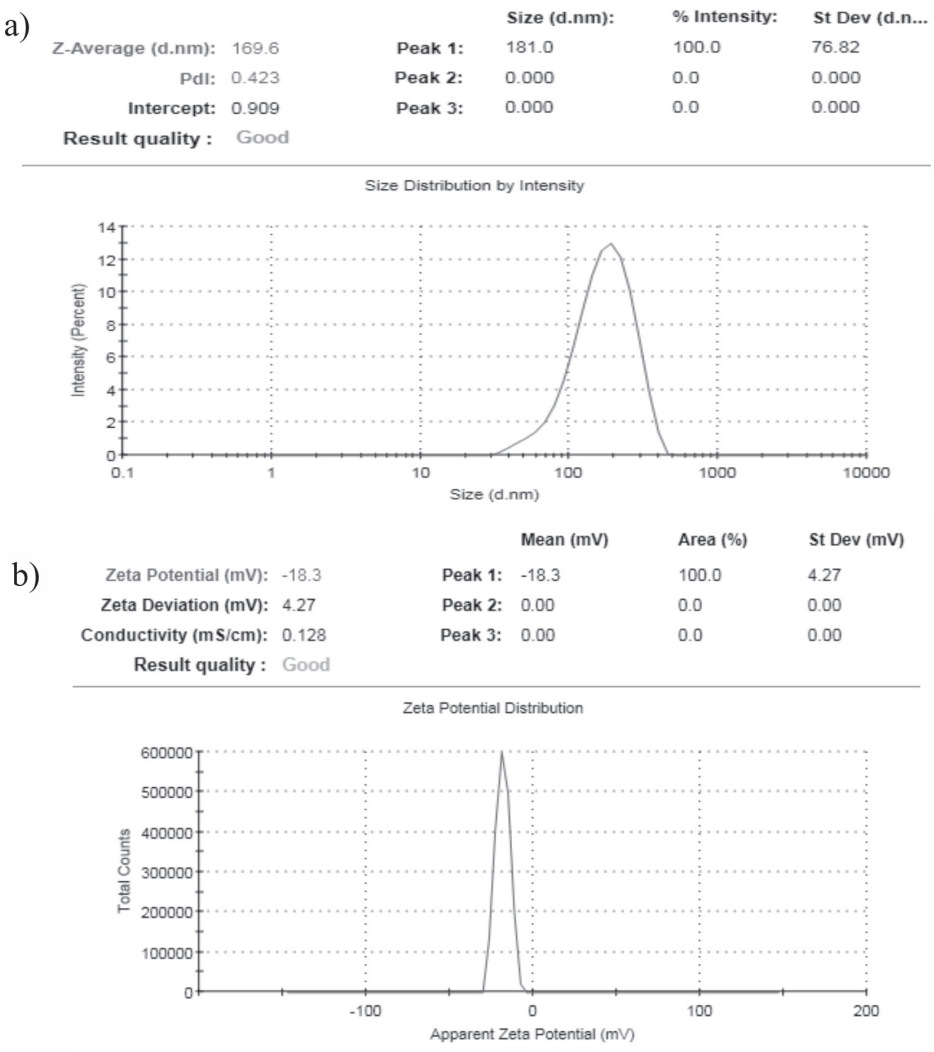

Fig. 7. a) Hydrodynamic diameter of ZnO NPs in aqueous solution, b) Zeta potential value of ZnO NPs.

Consequently, the combined effectiveness of the naturally occurring ZnO NPs at a concentration of 200 µg/disk was evaluated in combination with fluconazole (25 µg/disk) against the examined candidal pathogens. The antifungal mechanism was elucidated based on the capacity of ZnO NPs to penetrate the fungal membrane by diffusion and endocytosis. Zinc oxide nanoparticles disrupt mitochondrial activity inside the cytoplasm, leading to the generation of reactive oxygen species (ROS) and the release of zinc ions (Zn^{2+}). The excessive generation of ROS and zinc ions (Zn^{2+}) led to permanent DNA damage and the demise of cells [47]. The enhanced fungicidal efficacy of ZnO NPs in the current investigation might be ascribed

Table 3. Screening of antimicrobial activity of the bioinspired ZnONPs against candidal pathogens.

Candidal strains	ZnONPs (100 µg/disk)	ZnONPs (200 µg/disk)	Fluconazole (25 µg/disk)	Negative control
C. albicans	10.14±0.54 ^{a}	12.78±0.28 ^{a}	18.53±0.42 ^{a}	0.00±0.00
C. glabrata	00.00±0.00 ^{b}	10.61±0.47 ^{b}	0.00±0.00 ^{b}	0.00±0.00
C. parapsilosis	10.94±0.63 ^{a}	11.64±0.59 ^{c}	12.17±0.43 ^{c}	0.00±0.00
C. tropicalis	16.24±0.47 ^{c}	18.67±0.56 ^{d}	20.24±0.56 ^{d}	0.00±0.00
	MIC		MFC	
C. tropicalis	100 µg/ml		200 µg/ml	

Different superscript letters indicated that values were significantly different at $p \leq 0.05$.

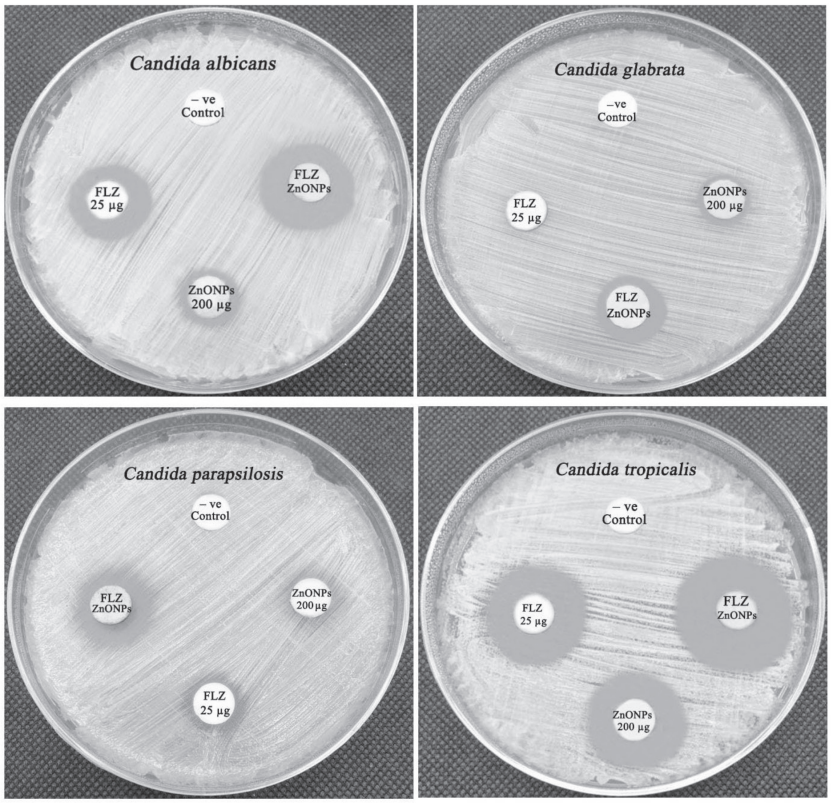

Fig. 8. Synergistic antifungal action of ZnO NPs with fluconazole against fungal pathogens.

to the diminutive size of the synthesized ZnO NPs. A prior report further affirmed that the antifungal activity of ZnO NPs is influenced by their size [48]. Other researchers have also observed a correlation between the size of particles and antimicrobial action [49]. The antifungal effects of ZnO nanoparticles may be attributed to their ability to generate reactive oxygen species, leading to a modification in the permeability of the cell membrane. This modification results in the release of lipids and proteins from the membrane, ultimately leading to the demise of microbial cells [50]. In a previous investigation, researchers explored how the size of ZnO nanoparticles influenced the survival of *C. albicans*. Their findings revealed that smaller particles demonstrated greater effectiveness in inhibiting fungal growth compared to larger particles [51]. The antifungal efficacy of biogenic ZnO NPs is associated with the internal production of diverse free radicals, including singlet oxygen, hydroxyl radicals, superoxide radicals, and nitric oxide radicals. These radicals have the ability to enter the nuclear membrane, resulting in DNA damage and possibly causing permanent chromosomal damage or cell death [52]. The suggested mode of action indicates that the fungicidal effect is accomplished by deactivating sulfhydryl groups in the fungal cell wall, leading to the generation of insoluble substances. This process finally culminates in the degradation of membrane-bound enzymes and lipids, leading to the demise of the cell [53]. The bioproduced ZnO nanoparticles, synthesized utilizing the *Prosopis farcta* plant, were reported to have antifungal properties against the *C. albicans* strain. The lowest inhibitory concentration was determined to be 128 µg/mL, while the fungicidal concentration was found to be 256 µg/mL [54]. Remarkably, the biogenic ZnO nanoparticles exhibited a greater level of antifungal activity against the *C. tropicalis* strain compared to what was reported before. This was shown by a relative MIC value of 100µg/ml, while the relative MFC was 200 µg/mL. The reason for this discrepancy might be attributed to the smaller particle size of ZnO NPs in the present study, which measured 27.92 nm. In contrast, the prior study reported that the biogenic ZnO NPs were hexagonal in shape and varied in size from 50 to 80 nm [55]. Previous research has found a link between the antimicrobial effect and the size of biogenic ZnO NPs. This association may be ascribed to the fact that smaller particles are more capable of penetrating microbial cells, hence exerting their fungicidal action against microbes [56]. The antifungal action of the environmentally friendly synthesized ZnO nanoparticles may be related to the presence of phytochemicals, such as alcohols, amines, alkenes, alkanes, and phenols, which are capped over the ZnO nanoparticles, as proven by FTIR analysis.

Synergistic Antifungal Action of Biogenic ZnO NPs with Fluconazole

The study examined the combined effectiveness of ZnO NPs and fluconazole antifungal drugs against

Table 4. Synergistic antifungal activity of bioinspired ZnONPs with fluconazole against the tested strains.

Candidal strains	ZnONPs (200 µg/disk)	Fluconazole (25 µg/disk)	FLZ (25 µg/disk) + ZnONPs (200 µg/disk)	Negative control	IFA
C. albicans	12.56±0.54[a]	18.14±0.36[a]	24.68±0.47[a]	0.00±0.00	0.85
C. glabrata	10.53±0.21[b]	00.00±0.00[b]	16.14±0.61[b]	0.00±0.00	NA
C. parapsilosis	11.12±0.45[c]	12.09±0.47[c]	17.86±0.23[c]	0.00±0.00	1.58
C. tropicalis	18.19±0.51[d]	20.52±0.67[d]	26.12±0.34[d]	0.00±0.00	0.62

Different superscript letters indicated that values were significantly different at $p \leq 0.05$.

the pathogenic fungal strains. The disc diffusion technique was used for this investigation (see Fig. 8). In this particular situation, ZnO NPs had the most significant combined impact with fluconazole in inhibiting the growth of the *C. glabrata* strain. The inhibitory zone diameter, compared to other treatments, was measured at 16.14±0.61 mm. However, it is worth noting that this strain has shown resistance to fluconazole. In addition, the bioinspired ZnO NPs exhibited a higher synergistic effect with fluconazole against the *C. parapsilosis* strain, as indicated by a relative IFA value of 1.58. However, moderate synergistic effects were observed against *C. albicans* and *C. tropicalis* strains, with relative IFA values of 0.85 and 0.62, respectively (Table 4). The synergistic antifungal activity might be attributed to the fact that both fluconazole and biogenic ZnO NPs target distinct cellular components. In this respect, fluconazole belongs to the azole antifungal group, which has its fungicidal mechanism of action via the inhibition of the 14α-lanosterol demethylase enzymes, creating a disruption in ergosterol production, a crucial cell membrane component. Consequently, the fungal cells undergo a reduction in ergosterol and an increase in harmful 14-methylated sterols, resulting in the breakdown and demise of the cells [57]. The fluconazole-induced disruption of the cell membrane allowed the biogenic ZnO NPs to enter the fungal cells. These nanoparticles then exerted their fungicidal effect by generating reactive oxygen species, which resulted in the disruption of fungal DNA, enzymes, and proteins. Ultimately, this led to cell death and the release of vital intracellular components [58]. The combined antifungal effect of biogenic ZnO nanoparticles and fluconazole has the potential to be used in the development of novel antifungal medications. This might help decrease the occurrence of drug-resistant candidal strains and enhance the effectiveness of conventional antifungal agents.

Investigation of Fungal Cell Deformations Using SEM Analysis

A scanning electron microscopy examination was used to study the morphological deformations of *C. albicans* cells treated with biogenic ZnO NPs. SEM images revealed that the outer membranes of the treated candidal cells exhibited wrinkles and the existence of pores (Fig. 9). These pores in the membranes of candidal cells resulted in the release of internal components, ultimately leading to the death of the fungal cells. Furthermore, treated cells were often larger in size, with uneven shapes and damaged cell walls. The rupturing and weakening of the cell wall, as well as the disintegration of the cytoplasmic membrane and its separation from the cell wall, demonstrated the anticandidal potential of ZnO nanoparticles [59]. *Candida albicans* control cells, on the other hand, were typically oval in shape with an intact cell membrane and cell wall [60].

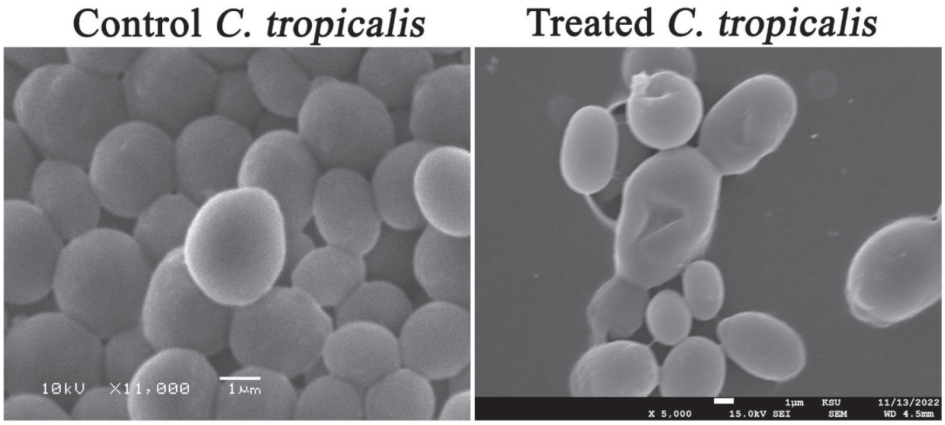

Fig. 9. The effect of biogenic ZnO NPs on candidal cells and deformations of *C. albicans* strain in the treated sample compared to control.

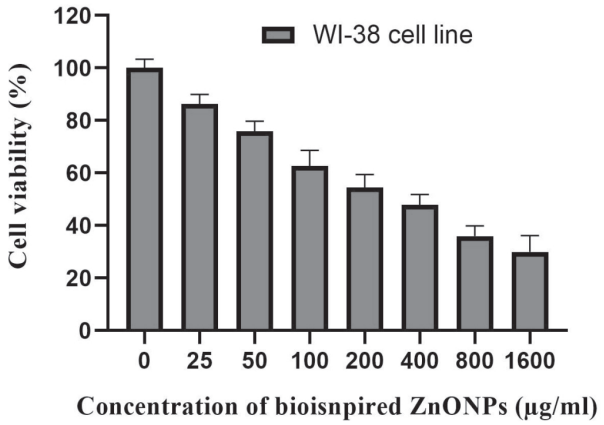

Fig. 10. Cell viability percentages at different concentrations of ZnO NPs.

Cytotoxicity Assay

A cytotoxicity assay was conducted on the WI-38 cell line (normal lung fibroblast cells) to explore the potential cytotoxic effects of varied concentrations of biosynthesized ZnO NPs and assess their safety for application. The cytotoxicity of these nanoparticles demonstrated a concentration-dependent pattern, with higher concentrations leading to decreased cell viability. Fig. 10 depicts minimal cytotoxicity in WI-38 cells exposed to low doses of biogenic ZnO NPs, with relative cell viability percentages of 86.39% and 75.64% at 25 and 50 µg/mL, respectively.

Linear regression analysis was conducted to determine the IC_{50} concentration of ZnO NPs, representing the concentration at which cell viability is reduced by 50%. The estimated IC_{50} value against normal lung fibroblast cells was 723.86 µg/mL. Notably, this concentration was ten times higher than the MIC concentration, indicating the safety of biogenic ZnO NPs. The results remained within the safe thresholds established by the U.S. National Cancer Institute, where a drug is considered hazardous if its IC_{50} value in early testing is less than 20 µg/mL [61]. Additionally, the U.S. Food and Drug Administration (FDA) has classified zinc oxide nanoparticles as safe, specifically placing them under the generally recognized as safe (GRAS) category [62].

Conclusions

The use of the aqueous seed extract from *T. foenum-graecum* facilitated the creation of biogenic ZnO nanoparticles with promising physicochemical characteristics. These nanoparticles displayed a hexagonal morphology, featuring an average diameter of 27.92 nm and a surface charge of -18.3 mV. The bioformulated zinc oxide nanoparticles exhibited significant antifungal activity against pathogenic Candida strains. Moreover, when combined with the fluconazole antifungal agent, the biogenic ZnO NPs demonstrated a synergistic antifungal effect against the tested candidal pathogens. This implies the potential for developing novel antifungal combinations to augment the efficacy of conventional antifungal agents and reduce the toxicity associated with single-drug administration. The combination of biogenic ZnO nanoparticles with fluconazole demonstrates strong synergistic efficacy, indicating their potential use in the development of effective antimicrobial pharmaceuticals such as ointments, mouthwash, creams, and lotions for the effective treatment of candidiasis.

Acknowledgments

The authors extend their appreciation to the Researchers Supporting Project number (RSPD2025R1105), King Saud University, Riyadh, Saudi Arabia.

Author Contributions

Mohamed Taha Yassin contributed to the writing and original draft preparation. Khadiga A. Hasan and Aayasha Negi contributed to the investigation, and data curation. Sara Mohamed contributed to the formal analysis of results. Mohamed Ragab AbdelGawwad and Fatimah O. Al-Otibi contributed to the reviewing, and editing.

Conflict of Interest

The authors declare no conflict of interest.

References

1. SHARMA M., CHAKRABARTI A. Candidiasis and Other Emerging Yeasts. Current Fungal Infection Reports. **17** (1), 15, **2023**.
2. OLIVA A., DE ROSA F.G., MIKULSKA M., PEA F., SANGUINETTI M., TASCINI C., VENDITTI M. Invasive Candida infection: epidemiology, clinical and therapeutic aspects of an evolving disease and the role of rezafungin. Expert Review of Anti-Infective Therapy. **21** (9), 957, **2023**.
3. RABAAN A.A., SULAIMAN T., AL-AHMED S.H., BUHALIQAH Z.A., BUHALIQAH A.A., ALYUOSOF B., ALFARESI M., AL FARES M.A., ALWARTHAN S., ALKATHLAN M.S., ALMAGHRABI R.S., ABUZAID A.A., ALTOWAILEB J.A., AL IBRAHIM M., ALSALMAN E.M., ALSALMAN F., ALGHOUNAIM M., BUEID A.S., AL-OMARI A., MOHAPATRA R.K. Potential Strategies to Control the Risk of Antifungal Resistance in Humans: A Comprehensive Review. Antibiotics. **12** (3), 608, **2023**.

4. LOCKHART S.R., CHOWDHARY A., GOLD J.A.W. The rapid emergence of antifungal-resistant human-pathogenic fungi. Nature Reviews Microbiology. **21** (12), 818, **2023**.
5. NGUYEN B.V.G., NGUYEN H.H.N., VO T.H., LE M.T., TRAN-NGUYEN V.K., VU T.T., NGUYEN, P. Prevalence and drug susceptibility of clinical Candida species in nasopharyngeal cancer patients in Vietnam. One Health. **18**, 100659, **2024**.
6. YASSIN M.T., MOSTAFA A.A., AL-ASKAR A.A., BDEER R. In vitro antifungal resistance profile of Candida strains isolated from Saudi women suffering from vulvovaginitis. European Journal of Medical Research. **25**, 1, **2020**.
7. YASSIN M.T., MOSTAFA A.A.F., AL-ASKAR A.A., AL-OTIBI F.O. Synergistic antifungal efficiency of biogenic silver nanoparticles with itraconazole against multidrug-resistant candidal strains. Crystals. **12** (6), 816, **2022**.
8. YASSIN M.T., MOSTAFA A.A.F., AL-ASKAR A.A., AL-OTIBI F.O. Facile green synthesis of zinc oxide nanoparticles with potential synergistic activity with common antifungal agents against multidrug-resistant candidal strains. Crystals. **12** (6), 774, **2022**.
9. PUUMALA E., FALLAH S., ROBBINS N., COWEN L.E. Advancements and challenges in antifungal therapeutic development. Clinical Microbiology Reviews. **0**(0), e00142, **2024**.
10. SRIVASTAVA R., RAWAT A.K.S., MISHRA M.K., PATEL A.K. Advancements in Nanotechnology for Enhanced Antifungal Drug Delivery: A Comprehensive Review. Infectious Disorders - Drug Targets. **24** (2), 24, **2024**.
11. KHAN I, SAEED K, KHAN I. Nanoparticles: Properties, applications and toxicities. Arabian Journal of Chemistry. **12** (7), 908, **2019**.
12. GOLD K., SLAY B., KNACKSTEDT M., GAHARWAR A.K. Antimicrobial activity of metal and metal-oxide based nanoparticles. Advances in Therapy. **1** (3), 1700033, **2018**.
13. ISLAM F., SHOHAG S., UDDIN M.J., ISLAM M.R., NAFADY M.H., AKTER A., MITRA S., ROY A., EMRAN T., CAVALU S. Exploring the Journey of Zinc Oxide Nanoparticles (ZnO-NPs) toward Biomedical Applications. Materials. **15** (6), 2160, **2022**.
14. BACHHAV K., GARDE A.S. Versatile synthesis of zinc oxide nanoparticles via chemical route: A review. Materials Today: Proceedings. **2023**.
15. DUAN H., WANG D., LI Y. Green chemistry for nanoparticle synthesis. Chemical Society Reviews. **44** (16), 5778, **2015**.
16. MADANI M., HOSNY S., ALSHANGITI D.M., NADY N., ALKHURSANI S.A., ALKHALDI H., AL-GAHTANY S.A., GHOBASHY M.M., GABER, G.A. Green synthesis of nanoparticles for varied applications: Green renewable resources and energy-efficient synthetic routes. Nanotechnology Reviews. **11** (1), 731, **2022.**
17. HANO C., ABBASI B.H. Plant-Based Green Synthesis of Nanoparticles: Production, Characterization and Applications. Biomolecules. **12** (1), 31, **2022**.
18. VERMA R., PATHAK S., SRIVASTAVA A.K., PRAWER S., TOMLJENOVIC-HANIC S. ZnO nanomaterials: Green synthesis, toxicity evaluation and new insights in biomedical applications. Journal of Alloys and Compounds. **876**, 160175, **2021**.
19. VIJAYAKUMAR S., VASEEHARAN B., SUDHAKARAN R., JEYAKANDAN J., RAMASAMY P., SONAWANE A., PADHI A., VELUSAMY P., ANBU P., FAGGIO C. Bioinspired Zinc Oxide Nanoparticles Using Lycopersicon esculentum for Antimicrobial and Anticancer Applications. Journal of Cluster Science. **30** (6), 1465, **2019**.
20. SURESH J., PRADHEESH G., ALEXRAMANI V., SUNDRARAJAN M., HONG S.I. Green synthesis and characterization of zinc oxide nanoparticle using insulin plant (Costus pictus D. Don) and investigation of its antimicrobial as well as anticancer activities. Advances in Natural Sciences: Nanoscience and Nanotechnology**. 9** (1), 015008, **2018**.
21. Irshad S., Salamat A., Anjum A.A., Sana S.; Saleem R.S.; Naheed A.; Iqbal A. Green tea leaves mediated ZnO nanoparticles and its antimicrobial activity. Cogent Chemistry. **4** (1), 1469207, **2018.**
22. RIZWANA H., ALWHIBI M.S., ALDARSONE H.A., AWAD M.A., SOLIMAN D.A., BHAT R.S. Green synthesis, characterization, and antimicrobial activity of silver nanoparticles prepared using Trigonella foenum-graecum L. leaves grown in Saudi Arabia. Green Processing and Synthesis. **10** (1), 421, **2021**.
23. KUMAR D., WANGKHEIRAKPAM R.S., RAHAL A., MALIK J.K. Fenugreek in Health and Disease. In: Gupta RC, Srivastava A, Lall R, editors. Nutraceuticals in Veterinary Medicine. Springer: Cham, Switzerland, pp. 25, **2019**.
24. YASSIN M.T., ELGORBAN A.M., AL-ASKAR A.A., SHOLKAMY E.N., AMEEN F., MANIAH K. Synergistic anticandidal activities of greenly synthesized ZnO nanomaterials with commercial antifungal agents against candidal infections. Micromachines. **14** (1), 209, **2023**.
25. YASSIN M.T., AL-ASKAR A.A., MANIAH K., AL-OTIBI F.O. Green synthesis of zinc oxide nanocrystals utilizing origanum majorana leaf extract and their synergistic patterns with colistin against multidrug-resistant bacterial strains. Crystals. **12** (11), 1513, **2022**.
26. MANIAH K. Anticandidal effectiveness of greenly synthesized zinc oxide nanoparticles against candidal pathogens. Journal of Environmental Science and Health, Part A. **58** (14), 1097-1110, **2023**.
27. CHAND P., KUMARI S., MONDAL N., SINGH S.P., PRASAD T. Synergism of Zinc Oxide Quantum Dots with Antifungal Drugs: Potential Approach for Combination Therapy against Drug Resistant Candida albicans. Frontiers in Nanotechnology. **3**, 624564, **2021**.
28. OVAIS M., KHALIL A.T., ISLAM N.U., AHMAD I., AYAZ M., SARAVANAN M., SHINWARI Z.K., MUKHERJEE S. Role of plant phytochemicals and microbial enzymes in biosynthesis of metallic nanoparticles. Applied Microbiology and Biotechnology. **102** (16), 6799, **2018**.
29. GITHALA C.K., TRIVEDI R. Review on synthesis method, biomolecules involved, size affecting factors and potential applications of silver nanoparticles. Biocatalysis and Agricultural Biotechnology. **54**,102912, **2023**.
30. SUPIN K.K., VASUNDHARA M. Green synthesis of ZnO nanoparticles from Neem and Eucalyptus leaves extract for photocatalytic applications. Materials Today: Proceedings. **92**, 787, **2023**.
31. SULTANA K.A., ISLAM M.T., SILVA J.A., TURLEY R.S., HERNANDEZ-VIEZCAS J.A., GARDEA-TORRESDEY J.L., NOVERON J.C. Sustainable synthesis of zinc oxide nanoparticles for photocatalytic degradation of organic pollutant and generation of hydroxyl radical. Journal of Molecular Liquids. **307**, 112931, **2020**.

32. PILLAI A.M., SIVASANKARAPILLAI V.S., RAHDAR A., JOSEPH J., SADEGHFAR F., RAJESH K., KYZAS G.Z. Green synthesis and characterization of zinc oxide nanoparticles with antibacterial and antifungal activity. Journal of Molecular Structure. **1211**, 128107, **2022**.
33. Fahaduddin, Bal T. Invitro- invivo evaluations of green synthesized zinc oxide (ZnO) nanoparticles using Ipomoea aquatica leaf extract as matric and fillers. Journal of the Mechanical Behavior of Biomedical Materials. **150**, 106330, **2024**.
34. VIMALA K., SUNDARRAJ S., PAULPANDI M., VENGATESAN S., KANNAN S. Green synthesized doxorubicin loaded zinc oxide nanoparticles regulates the Bax and Bcl-2 expression in breast and colon carcinoma. Process Biochemistry. **49**, 160, **2024**.
35. AL-AJMI M.F., HUSSAIN A., ALSHARAEH E., AHMED F., AMIR S., ANWAR M.S., SIDDIQUI M.A., AL-KHEDHAIRY A.A., KOO B.H. Green Synthesis of Zinc Oxide Nanoparticles Using Alstonia Macrophylla Leaf Extract and Their In-Vitro Anticancer Activity. Science of Advanced Materials. **10**, 349, **2018**.
36. DEMISSIE M.G., SABIR F.K., EDOSSA G.D., GONFA B.A. Synthesis of Zinc Oxide Nanoparticles Using Leaf Extract of Lippia adoensis (Koseret) and Evaluation of Its Antibacterial Activity. Journal of Chemistry. **2020**, e7459042, **2020**.
37. EL-KAHKY D., ATTIA M., EASA S.M., AWAD N.M., HELMY E.A. Interactive Effects of Biosynthesized Nanocomposites and Their Antimicrobial and Cytotoxic Potentials. Nanomaterials. **11**, 903, **2021**.
38. ADEGOKE H.I., GBENGA A.A. Bio-Assisted Synthesis of Zinc Oxide Nanoparticles from Mimosa pudica Aqueous Leave Extract: Structure and Antibacterial Activity. Chemistry Africa. **6** (3), 1283, **2023**.
39. KORDE S.A., THOMBRE P.B., DIPAKE S.S., SANGSHETTI J.N., RAJBHOJ A.S., GAIKWAD S.T. Neem gum (Azadirachta indicia) facilitated green synthesis of TiO2 and ZrO2 nanoparticles as antimicrobial agents. Inorganic Chemistry Communications. **153**,110777, **2023**.
40. PREM P., NAVEENKUMAR S., KAMARAJ C., RAGAVENDRAN C., PRIYADHARSAN A., MANIMARAN K., ALHARBI N.S., RAROKAR N., CHERIAN T., SUGUMAR V., THIRUVENGADAM M., KUMARASAMY V., SUBRAMANIYAN V. Valeriana jatamansi root extract a potent source for biosynthesis of silver nanoparticles and their biomedical applications, and photocatalytic decomposition. Green Chemistry Letters and Reviews. **17**, 2305142, **2024**.
41. MENAZEA A.A., ISMAIL A.M., SAMY A. Novel Green Synthesis of Zinc Oxide Nanoparticles Using Orange Waste and Its Thermal and Antibacterial Activity. Journal of Inorganic and Organometallic Polymers and Materials. **31**, 4250, **2021**.
42. KONAPPA N., JOSHI S.M., DHAMODARAN N., KRISHNAMURTHY S., BASAVARAJU S., CHOWDAPPA S., JOGAIAH S. Green synthesis of Callicarpa tomentosa routed zinc oxide nanoparticles and their bactericidal action against diverse phytopathogens. Biomass Conversion and Biorefinery. **2022.**
43. ELUMALAI K., VELMURUGAN S. Green synthesis, characterization and antimicrobial activities of zinc oxide nanoparticles from the leaf extract of Azadirachta indica (L.). Applied Surface Science. **345**, 329, **2015**.
44. ABDULLAH F.H., ABU BAKAR N.H.H., ABU BAKAR M. Comparative study of chemically synthesized and low temperature bio-inspired Musa acuminata peel extract mediated zinc oxide nanoparticles for enhanced visible-photocatalytic degradation of organic contaminants in wastewater treatment. Journal of Hazardous Materials. **406**, 124779, **2021**.
45. BARZINJY A.A., AZEEZ H.H. Green synthesis and characterization of zinc oxide nanoparticles using Eucalyptus globulus Labill. leaf extract and zinc nitrate hexahydrate salt. SN Applied Sciences. **2** (5), 991, **2020**.
46. ZAFAR S., ASHRAF A., IJAZ M.U., MUZAMMIL S., SIDDIQUE M.H., AFZAL S., ANDLEEB R., AL-GHANIM K.A., AL-MISNED F., AHMED Z., MAHBOOB S. Eco-friendly synthesis of antibacterial zinc nanoparticles using Sesamum indicum L. extract. Journal of King Saud University – Science. **32** (1), 1116, **2020**.
47. CHAUHAN A.K., KATARIA N., GARG V.K. Green fabrication of ZnO nanoparticles using Eucalyptus spp. leaves extract and their application in wastewater remediation. Chemosphere. **247**, 125803, **2020**.
48. HAMED R., OBEID R.Z., ABU-HUWAIJ R. Plant mediated-green synthesis of zinc oxide nanoparticles: An insight into biomedical applications. Nanotechnology Reviews. **12**, 20230112, **2023**.
49. RAJIV P., RAJESHWARI S., VENCKATESH R. Bio-Fabrication of zinc oxide nanoparticles using leaf extract of Parthenium hysterophorus L. and its size-dependent antifungal activity against plant fungal pathogens. Spectrochimica Acta, Part A: Molecular and Biomolecular Spectroscopy. **112**, 384–387, **2013**.
50. JEONG Y., LIM D.W., CHOI J. Assessment of Size-Dependent Antimicrobial and Cytotoxic Properties of Silver Nanoparticles. Advances in Materials Science and Engineering. **2014**, e763807, **2014**.
51. HAJA HAMEED A.S., KARTHIKEYAN C., SENTHIL KUMAR V., KUMARESAN S., SASIKUMAR S. Effect of Mg^{2+}, Ca^{2+}, Sr^{2+} and Ba^{2+} metal ions on the antifungal activity of ZnO nanoparticles tested against Candida albicans. Materials Science and Engineering: C. **52**, 171, **2015**.
52. LIPOVSKY A., NITZAN Y., GEDANKEN A., LUBART R. Antifungal activity of ZnO nanoparticles—the role of ROS mediated cell injury. Nanotechnology. **22**, 105101, **2011**.
53. MOSTAFA M., AMAL A., ALMOAMMAR H., ABD-ELSALAM K.A. Nanoantimicrobials Mechanism of Action. In: Abd-Elsalam KA, Prasad R, Eds.; Nanobiotechnology Applications in Plant Protection. Springer: Cham, Switzerland, pp. 281, **2018**.
54. PAL A., GOSWAMI R., ROY D.N. A critical assessment on biochemical and molecular mechanisms of toxicity developed by emerging nanomaterials on important microbes. Environmental Nanotechnology, Monitoring and Management. **16**, 100485, **2021**.
55. MIRI A., MAHDINEJAD N., EBRAHIMY O., KHATAMI M., SARANI M. Zinc oxide nanoparticles: Biosynthesis, characterization, antifungal and cytotoxic activity. Materials Science and Engineering: C. **104**, 109981, **2019**.
56. BINDHU M.R., UMADEVI M. Antibacterial activities of green synthesized gold nanoparticles. Materials Letters. **120**, 122, **2014**.
57. KATHIRAVAN M.K., SALAKE A.B., CHOTHE A.S., DUDHE P.B., WATODE R.P., MUKTA M.S., GADHWE S. The biology and chemistry of antifungal agents: A review. Bioorganic & Medicinal Chemistry. **20**, 5678, **2012**.

58. HUQ M.A., APU M.A.I., ASHRAFUDOULLA M., RAHMAN M.M., PARVEZ M.A.K., BALUSAMY S.R., AKTER S., RAHMAN M. Bioactive ZnO Nanoparticles: Biosynthesis, Characterization and Potential Antimicrobial Applications. Pharmaceutics. **15** (11), 2634, **2023**.
59. JALAL M., ANSARI M.A., ALI S.G., KHAN H.M., REHMAN S. Anticandidal activity of bioinspired ZnO NPs: effect on growth, cell morphology and key virulence attributes of Candida species. Artificial Cells, Nanomedicine, and Biotechnology. **46**, 912, **2018**.
60. ANSARI M.A., ASIRI S.M.M. Green synthesis, antimicrobial, antibiofilm and antitumor activities of superparamagnetic γ-Fe2O3 NPs and their molecular docking study with cell wall mannoproteins and peptidoglycan. International Journal of Biological Macromolecules. **28**, 44, **2021**.
61. LAGUNES-CASTRO M.S., TRIGOS Á., LÓPEZ-MONTEON A., MENDOZA G., RAMOS-LIGONIO A. Cytotoxic activity and induction of inflammatory mediators of the methanol:chloroform extract of Fusarium moniliforme. Revista Iberoamericana de Micología. **32**, 235, **2015**.
62. SMIJS T.G., PAVEL S. Titanium dioxide and zinc oxide nanoparticles in sunscreens: focus on their safety and effectiveness. Nanotechnology, Science and Applications. **4**, 95, **2011**.